INSTITUT DE FRANCE
Académie des sciences

Comptes Rendus

Chimie

Mohammad Mazloum-Ardakani and Rezvan Arazi

Enhancement of photovoltaic performance using a novel photocathode based on poly(3,4-ethylenedioxythiophene)/Ag–CuO nanocomposite in dye-sensitized solar cells

Volume 23, issue 2 (2020), p. 105-115

Published online: 19 June 2020

https://doi.org/10.5802/crchim.7

Les Comptes Rendus. Chimie *sont membres du*
Centre Mersenne pour l'édition scientifique ouverte
www.centre-mersenne.org
e-ISSN : 1878-1543

Comptes Rendus
Chimie
2020, 23, nº 2, p. 105-115
https://doi.org/10.5802/crchim.7

Full paper / *Mémoire*

Enhancement of photovoltaic performance using a novel photocathode based on poly(3,4-ethylenedioxythiophene)/Ag–CuO nanocomposite in dye-sensitized solar cells

Mohammad Mazloum-Ardakani *, [a] **and Rezvan Arazi** [a]

[a] Department of Chemistry, Faculty of Science, Yazd University, Yazd, 89195-741, I.R. Iran.

E-mail: mazloum@yazd.ac.ir (M. Mazloum-Ardakani).

Abstract. A novel counter electrode (CE) based on a silver and copper oxide nanocomposite is developed and characterized by XRD and FE-SEM. A polymeric system containing poly(3,4-ethylenedioxythiophene) (PEDOT) is employed as the conductive polymer to prepare a transparent CE for a dye-sensitized solar cell (DSSC) device. Electrochemical analysis is used to study the catalytic activity of the reduction of triiodide ions in different DSSC-based CEs. To study the effect of photoelectrode modification on charge-transfer resistance, alternating current impedance spectroscopy is carried out. Power conversion efficiency and short-circuit current density (J_{SC}) increase from 8.01% to 9.06% and 16.18 to 17.79 mA/cm^2, respectively, due to the significantly improved electrical conductivity and electrocatalytic activity of the novel PEDOT/Ag–CuO nanocomposite-based CE.

Keywords. Counter electrode, Alternating current impedance spectroscopy, Dye-sensitized solar cells, CuO nanocomposite.

Manuscript received 1st October 2019, revised and accepted 5th November 2019.

1. Introduction

The excessive consumption of fossil fuels and the concern that they will be depleted have led researchers to look for renewable energy sources [1]. Photovoltaic phenomena are the most important among renewable energy sources as solar energy is abundant [2]. Sunlight is converted directly into electricity by a solar cell device through photovoltaic phenomena. Solar cells are studied in four generations [3–5]. Crystalline silicon wafer solar cells and thin-film solar cells belong to the first and the second generation, respectively. Nanocrystal and photoelectrochemical solar cells are referred to as the third generation. In addition, multi-junction technology and polymer solar cells are classified as the fourth generation. Dye-sensitized solar cells (DSSCs) belong to the third generation. They convert sunlight into electricity and thus overcome the fundamental limi-

* Corresponding author.

tations of efficiency conversion in single-junction devices. They are made from environment-friendly and cheap materials [6]. The DSSCs are a low-cost alternative to a conventional photovoltaic system based on wafer silicon or compound semiconductor devices. A DSSC is made of a photoanode, a redox couple (I_3^-/I^-) in the liquid electrolyte, a dye sensitizer adsorbed on mesoporous TiO_2 and a counter electrode (CE), the latter catalyzes electrolyte regeneration [7]. In DSSCs, Pt has good electrocatalytic activity (ECA) toward the reduction of I_3^-, and it is usually utilized as the photocathode. Because of its high cost, Pt-free materials such as inorganic transition metals [8], carbon materials [9] and conducting polymers [10] have attracted interest as a substitute for CEs due to their special properties. Conductive polymers were developed in 1977 by the discovery of the first conducting organic polymer, polyacetylene [11]. Polypyrrole, polyaniline, poly(3,4-ethylenedioxythiophene) (PEDOT) and polythiophene are some of the clearest examples of conductive polymers. PEDOT is a highly transparent, electrochemically active and conductive polymer that is used as a photocathode owing to its high surface roughness and good thermal stability [12].

In the past decades, advances in nanotechnology and nanoscience have expanded the possibilities for employing nanoparticles (NPs) in various fields: (1) metal/oxide nanoparticles, (2) carbon nanotubes, (3) graphene and (4) carbon nanofibers [13–15]. Metals such as nickel, manganese, zinc and copper have gained interest owing to their enormous advantages such as electron transfer capabilities, good ECA, large surface areas and easy accessibility [16]. Among these metal oxides, CuO-based materials as a p-type semiconductor have been explored extensively because of their band gap (1.2 eV) and easy sensitization [17].

In this study, a novel CE-based PEDOT/Ag–CuO nanocomposite was fabricated and characterized utilizing various techniques. Moreover, the *J–V* characteristic was used to study the effect of the new CE on the conversion efficiency of DSSCs. In this paper, electrocatalytic properties and charge-transfer resistance between redox species and different CEs such as platinum, PEDOT and PEDOT/Ag–CuO nanocomposite based CEs were investigated. Subsequently, photovoltaic parameters were studied and summarized.

2. Experimental section

2.1. *Materials*

Iodine (I_2), 4-tertiary butylpyridine (4-TBP), sodium borohydride, and acetic acid were obtained from Merck Chemical Co. 3,4-ethylenedioxythiophene (EDOT, 97%), titanium (IV) isopropoxide, ethyl cellulose, terpineol, guanidinium thiocyanate (GuSCN, ≥99.9%), acetonitrile (AN), anhydrous lithium iodide (LiI) and lithium perchlorate ($LiClO_4$) were ordered from Sigma-Aldrich and used as received. 1-methyl-3-propyl imidazolium iodide (MPII), platinum (IV) chloride ($PtCl_4$), $Cu(NO_3)_2.3H_2O$ and $AgNO_3$ were obtained from Fluka. The dye sensitizer [cis-dithiocyanate-N, N′-bis-(4-carboxylate-4-tetrabutylammonium carboxylate-2, 2′-bipyridine) ruthenium (II) (N719)] was bought from Solaronix S.A., Aubonne, Switzerland. Fluorine-doped SnO_2 glass (FTO), 2 mm in thickness, with a sheet resistance 12 Ω/square, was used as a substrate for blading the lab-made TiO_2 paste.

2.2. *Synthesis of Ag–CuO nanocomposite*

The Ag–CuO nanocomposite was obtained by the addition of 40 mL of 0.8 M sodium borohydride to a $AgNO_3$/Cu $(NO_3)_2$ mixture solution [6.80 mL of 0.88 M Cu $(NO_3)_2.6H_2O$ and 6.80 mL of 0.42 M $AgNO_3$ aqueous solutions] and stirred at 25 °C for 4 h to form a homogeneous precipitate. Subsequently, to remove the unreacted material, the precipitate was filtered, washed with deionized water and dried at 40 °C. Finally, the nanocomposite was annealed at 400 °C for 3 h to convert copper in the nanocomposite to CuO. The product obtained is the Ag–CuO nanocomposite.

2.3. *Preparation of different kinds of counter electrodes*

The FTO glass substrates used for the CEs were washed with detergents, water, and acetone and HCl/ethanol solution in an ultrasonic bath to remove iron contamination. Before that, the Pt, PEDOT, and PEDOT/Ag–CuO nanocomposite-based CEs were fabricated as described in the following steps. The Pt-based photocathodes were prepared

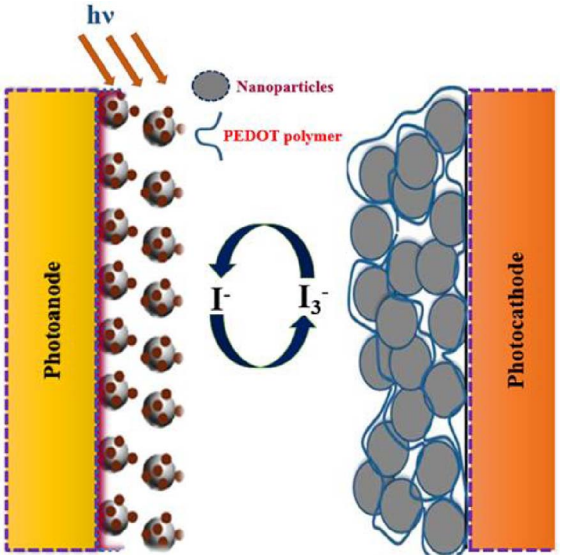

Scheme 1. Schematic illustration of how to place PEDOT/nanocomposite on the counter electrode.

by dropping a 5 mM $PtCl_4$ solution in isopropanol on the FTO glass substrates and then firing in a furnace at about 385 °C for about 15 min [18], whereas PEDOT and PEDOT/Ag–CuO nanocomposite based CEs were prepared by the electropolymerization of EDOT at 1.2 V (versus Ag/Ag^+ reference electrode) for 50 s with a three-electrode system in an acetonitrile solution [Ag–CuO nanocomposite (1.0 mg/mL) + EDOT (10 mM) at room temperature, Scheme 1)]. For comparison, PEDOT CE was prepared in $LiClO_4$ (0.1 M) without the Ag–CuO nanocomposite.

2.4. *Assembling of DSSCs based on different counter electrodes*

After cleaning the FTO glass substrates using an ultrasonic bath containing water and acetone (15 min), they were treated with $TiCl_4$ (40 mM) for 30 min at 70 °C ($TiCl_4$ pre-treatment). The lab-made TiO_2 paste [19] was spread onto the substrates to prepare photoanode electrodes with an optimized thickness. Then the prepared TiO_2 electrodes were immersed into the 40 mM $TiCl_4$ solution and heated at 70 °C for 30 min to improve electrical contact and adhesion ($TiCl_4$ post-treatment) and then sintered at 500 °C for 30 min. The active area of electrodes was selected at 0.16 cm^2. After sintering, the electrodes were immersed in a 5×10^{-4} M solution of N719 dye containing acetonitrile and tertiary butanol (1:1) for 21 h. The electrolyte solution has an optimized composition of LiI (0.6 M), I_2 (0.05 M), 4-TBP (0.5 M), GuSCN (0.1 M) and MPII (0.45 M) in an organic solvent. The electrolyte solution was injected into the different CEs through a hole and the photoelectrodes were physically sandwiched together using cell holders.

2.5. *Characterization of assembled DSSCs*

The current density–voltage parameters were obtained by a sunlight simulator equipped with a 450 W Xe lamp as a light source and a water-based IR filter and AM1.5 filter. Also, a potentiostat/galvanostat IVIUM instrument was used to characterize different DSSC-based CEs. To study the charge transport resistance between the redox species and the different CEs (PEDOT, PEDOT/Ag–CuO nanocomposite and Pt), alternating current (AC) impedance spectroscopy measurements were performed using an IVIUM instrument with Z-view software in the frequency range 0.1 Hz–0.3 MHz with two identical CEs. Tafel polarization analysis was carried out by a similar method as the impedance measurements and conducted at a scan rate of 20 mV/s. To study the ECA of the different CEs toward I_3^- reduction, cyclic voltammetry (CV) was carried out in an acetonitrile solution [LiI (0.01 M), $LiClO_4$ (0.1 M), I_2 (0.001 M)] using a three-electrode setup [potential range (−0.6 to 1.4), scan rate (50 mV/s)]. The XRD patterns of products were obtained by monochromatized Cu Kα radiation and X'PertPro diffractometer. A Mira 3-XMU field emission scanning electron microscope was used to examine the surface morphology of different CEs.

3. Results and discussion

3.1. *Field emission scanning electron microscopy (FE-SEM)*

The morphologies of PEDOT, Ag–CuO nanocomposite and PEDOT/Ag–CuO nanocomposite were examined using FE-SEM (Figure 1). As shown in Figure 1a, the FE-SEM image of electropolymerized PEDOT (50 s) on the FTO substrate shows a rougher

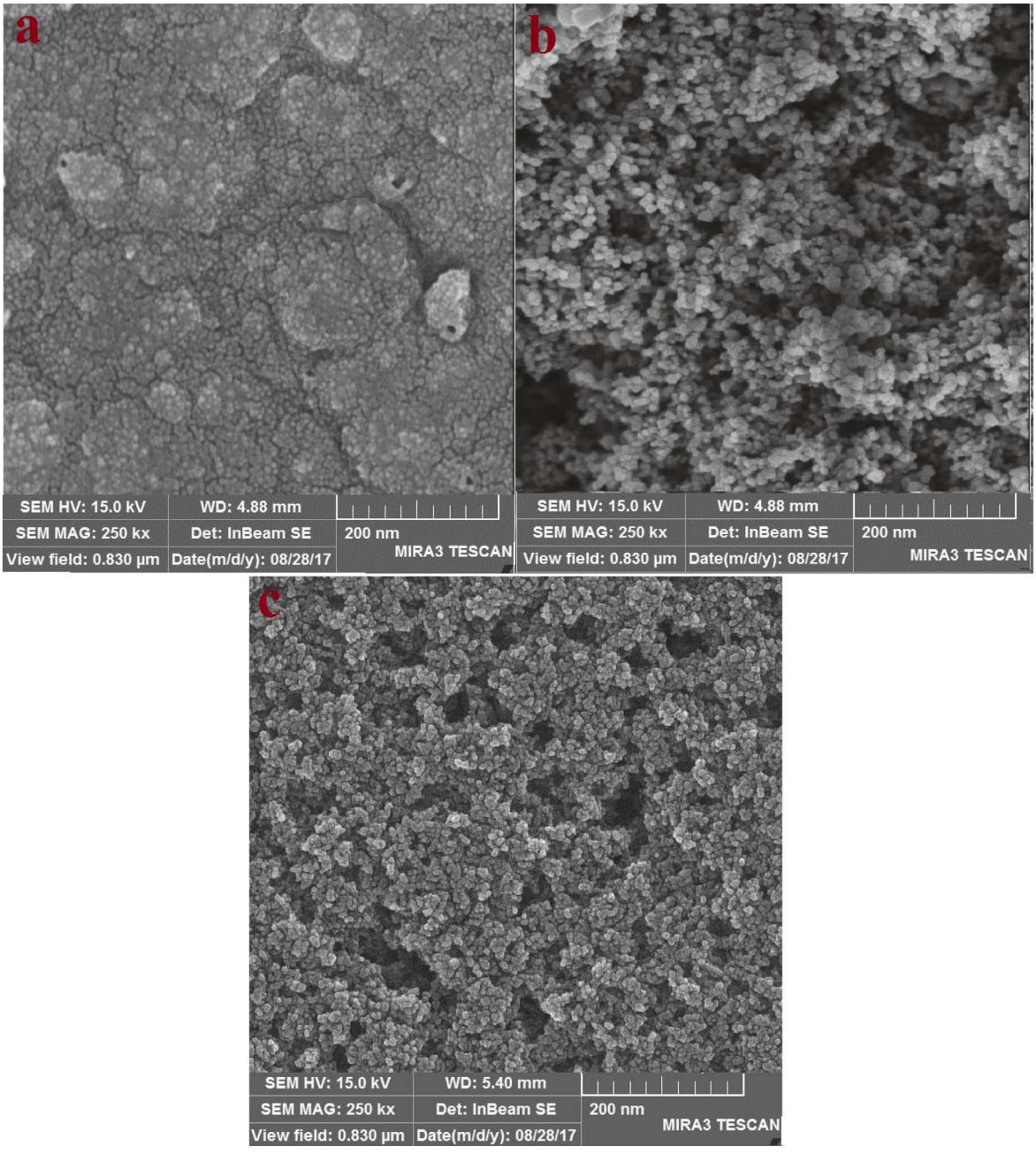

Figure 1. FE-SEM images (top view) of (a) PEDOT on the FTO substrate with polymerization time 50 s, (b) Ag–CuO nanocomposite and (c) PEDOT/Ag–CuO nanocomposite.

surface and a densely granular morphology. This result was in accordance with previously published studies [10,20]. In addition, the morphology of the as-synthesized Ag–CuO nanoparticles was studied by the FE-SEM technique. Figure 1b shows the FE-SEM image of the Ag–CuO nanoparticles, which are porous spherical nanoparticles suitable for the adsorption of triiodide ions. It shows a homogeneous

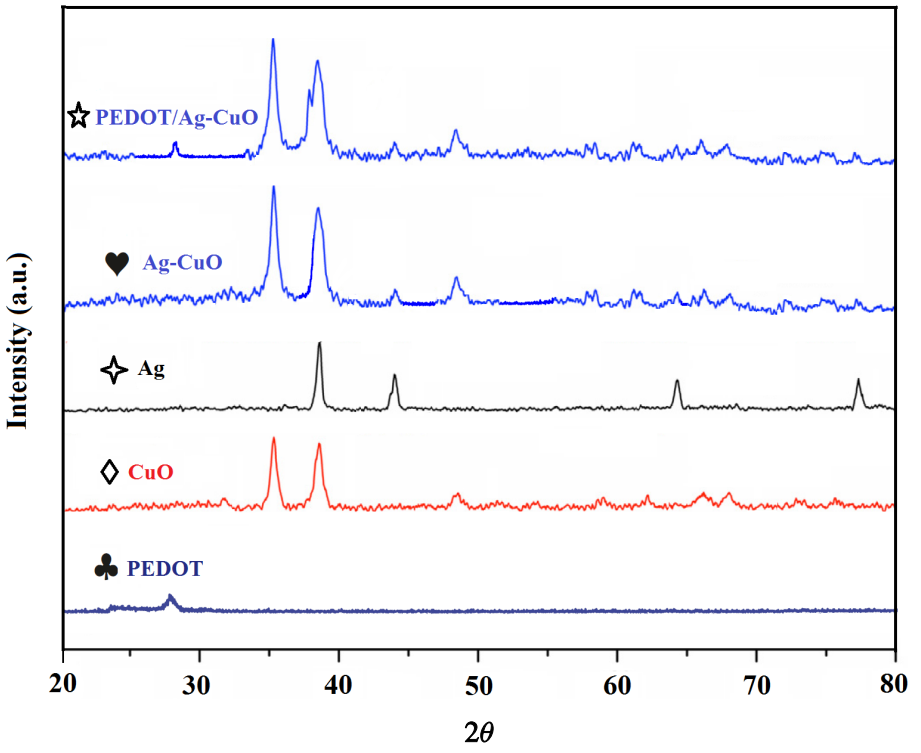

Figure 2. X-ray diffraction patterns of PEDOT with polymerization time 50 s, CuO NPs, Ag NPs, Ag–CuO nanocomposite, and PEDOT/Ag–CuO nanocomposite (PEDOT → ♣, CuO NPs → ♢, Ag NPs → ✧, Ag–CuO nanocomposite → ♡, and PEDOT/Ag–CuO nanocomposite → ☆).

distribution of grain-like crystals at the expected sizes, contributing to the increase in material surface area. Although the average particle sizes of the two nanoparticles look similar (about 40–50 nm), the CuO particles are uniform and regular in shape and size contrary to Ag nanoparticles. The electrochemical deposition of PEDOT (50 s) onto the porous templates to produce the novel PEDOT/Ag–CuO nanocomposite (Figure 1c) shows a mixture of dense granular and porous spherical nanoparticles. However, PE-DOT is distributed more uniformly throughout the film than in Figure 1a and wraps firmly over the nanoparticles. This result indicates a synergistic effect of both materials resulting in more active sites being exposed for triiodide reduction and subsequently achieving enhanced ECA and high power conversion efficiency (PCE). Furthermore, the high surface roughness structure of the PEDOT polymer in comparison with the other polymers leads to improved ECA and conversion efficiency [12].

3.2. *X-ray diffraction (XRD)*

The crystal structures of Ag, CuO, Ag–CuO, PEDOT and PEDOT/Ag–CuO nanocomposite were analyzed by powder XRD (Figure 2). The characteristic peaks at 38.4° (111), 44.9° (200), 64.8° (220) and 78.9° (311) are associated with monoclinic Ag (JCPDS 04-0783). All the diffraction peaks at 2θ = 32.54° (110), 35.09° (−111), 38.70° (111), 48.77° (−202), 53.48° (020), 58.29° (202), 61.65° (−113), 66.28° (−311) and 68.14° (113) can be attributed to the copper oxide phase. The XRD patterns of $AgNO_3$/$Cu(NO_3)_2$/PEDOT after the reduction process display well-defined diffraction peaks, corresponding to the Ag/CuO nanostructure. Actually, the reduction by hydrazine has effectively converted $AgNO_3$ and $Cu(NO_3)_2$ to Ag and CuO NPs in the test solution. A characteristic peak at approximately $2\theta \sim 27°$ [21] corresponds to the interchain planar ring stacking in all conducting polymers. In this study, PEDOT also exhibits a peak at

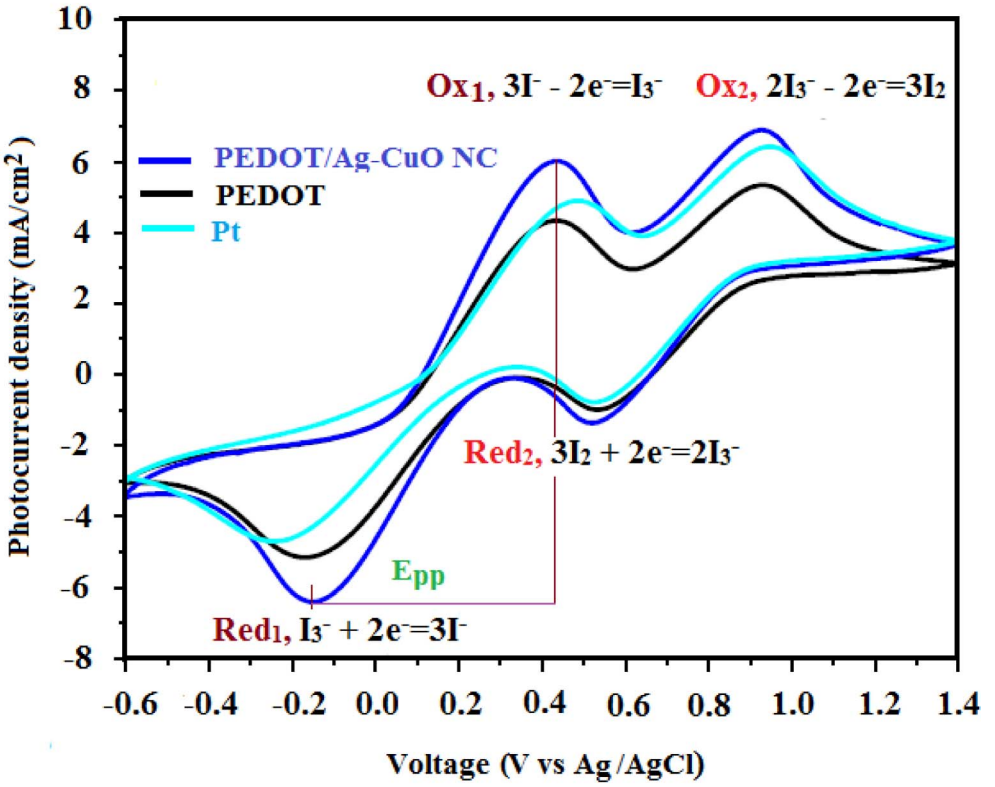

Figure 3. (a) Cyclic voltammograms obtained for PEDOT, PEDOT/Ag–CuO nanocomposite and Pt CE based counter electrodes in a three-electrode system at a scanning rate of 50 mV/s from 0.6 to +1.4 V for the oxidation and reduction of I^-/I_3^-.

26.2° (107), which is attributed to interchain planar ring stacking (JCPDS 00-048-1449). PEDOT/Ag–CuO nanocomposite diffraction peaks at 26.2° (107), 35.09° (−111) and 38.70° (111) show that the novel PEDOT/Ag–CuO nanocomposite was deposited on the substrate successfully and corresponds to all the peaks from PEDOT, Ag and CuO, indicating that all materials were present in the novel nanocomposite.

3.3. *Cyclic voltammetry*

Since the CE in the DSSC is responsible for catalyzing the regeneration of I^- from I_3^- ($I_3^- + 2e^- \rightarrow 3I^-$) [19], to understand whether the PEDOT/Ag–CuO nanocomposite CE is suitable for improving the electrocatalysis of different DSSCs, electrochemical properties of as-synthesized PEDOT, PEDOT/Ag–CuO nanocomposite and platinum were measured using CV. Figure 3 presents the two sets of redox peaks that are attributed to iodide–triiodide oxidation (1) and triiodide–iodine reduction (2).

$$3I^- \rightarrow I_3^- + 2e^-, \quad 2I_3^- \rightarrow 3I_2 + 2e^- \qquad (1)$$

$$I_3^- + 2e^- \rightarrow 3I^-, \quad 3I_2 + 2e^- \rightarrow 2I_3^- \qquad (2)$$

It was found that the peak current density (I_{peak}, Ip) and the peak-to-peak separation ($E_{peak-to-peak}$, Epp) are the two key parameters for evaluating the CE catalytic activities [22]. The cathodic peak current (Ipc) relates to I_3^- reduction and the anodic peak current (Ipa) relates to I^- oxidation in an acetonitrile-based electrolyte solution containing I_2 (0.001 M), $LiClO_4$ (0.1 M) and LiI (0.01 M). The Epp of the cathodic and anodic currents is inversely proportional to k_{redox}, while the Ipc is directly related to the CE ability to reduce I_3^- ions. The importance of I_3^- to I^- reduction corresponds to the electron transfer process and the electrocatalytic activation at the interface of the

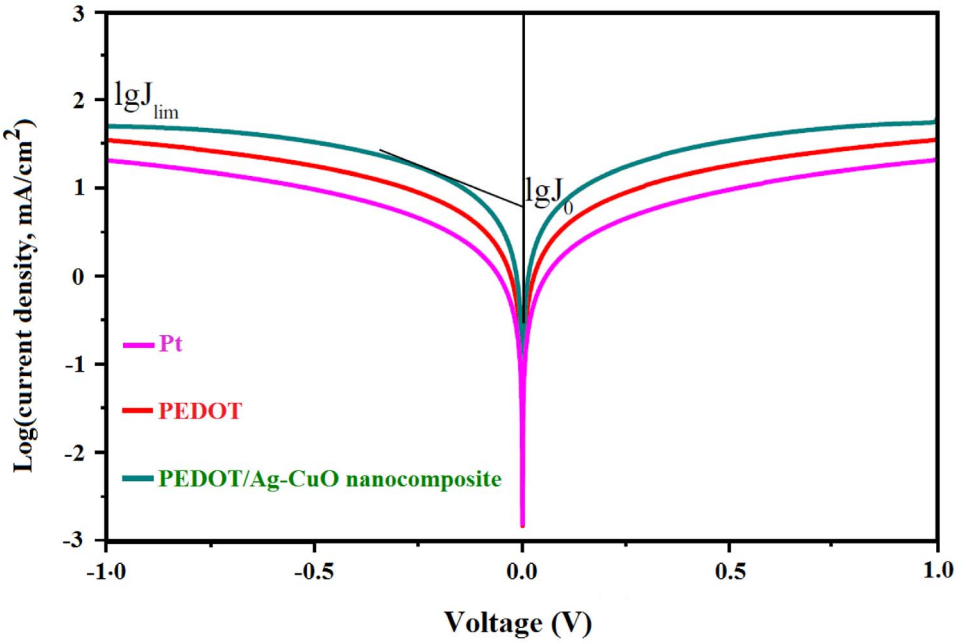

Figure 4. Tafel curves of the symmetric cells prepared by PEDOT, PEDOT/Ag–CuO nanocomposite and Pt CEs.

CE/electrolyte in the different DSSC devices. The Epp for PEDOT/Ag–CuO nanocomposite CE is ~560 mV, which is lower than that of the other two CEs (Epp of PEDOT CE ~ 590 mV and Pt CE ~680 mV), indicating a larger charge transfer for the PEDOT/Ag–CuO nanocomposite CE compared to the Pt CE. Compared with Pt, the PEDOT/Ag–CuO nanocomposite CE generates a larger cathodic photocurrent density (J_{Red1} = −6.50 mA/cm^2) than the other two electrodes (J_{Red1} = −5.20 mA/cm^2 for the PEDOT CE and −4.80 mA/cm^2 for Pt CE), suggesting the effective reduction of more adsorbed I_3^- ions on the novel PEDOT/Ag–CuO nanocomposite CE than on the Pt CE (larger active surfaces) [23]. Both the enhancement of Ipc and the Epp reduction indicate the excellent ECA of the PEDOT/Ag–CuO nanocomposite CE toward the I_3^-/I^- redox reaction [16]. This improves the photovoltaic performance of DSSCs, which enhances the electrocatalytic behavior for I_3^- reduction and provides a highly active area for more efficient and faster reactions of redox couples at the novel nanocomposite CE [24]. These results are accompanied by the Tafel polarization analysis, AC impedance measurements and *J*–*V* characteristics for the different DSSC-based CEs.

3.4. *Tafel polarization analysis*

Figure 4 compares the Tafel polarization curves for the different kinds of CEs to study the charge-transfer kinetics at the interface of the CE/electrolyte. The exchange current density (J_0) reveals the ability of photocathodes to facilitate and simplify redox reaction at the CE/electrolyte interfacial surface. A higher J_0 leads to a lower charge-transfer resistance R_{CT}, resulting in a higher photocurrent. According to (3) [25], R_{CT} is inversely proportional to J_0. Thus a good CE should have a lower R_{CT}:

$$J_0 = \mathrm{RT}/nFR_{ct}, \tag{3}$$

where n is the number of electrons involved in the redox reaction; R, T and F are the gas constant, the temperature and the Faraday constant, respectively. From the Tafel polarization curves, the slope of the polarization branch for the novel PEDOT/Ag–CuO nanocomposite represents the best value in comparison to those of the other two CEs (PEDOT and Pt CE), indicating that nanocomposite-based DSSCs exhibit high electroactivity in I_3^- reduction. A comparison of J_0 among three different kinds of counter electrolytes indicates that the new nanocomposite-based

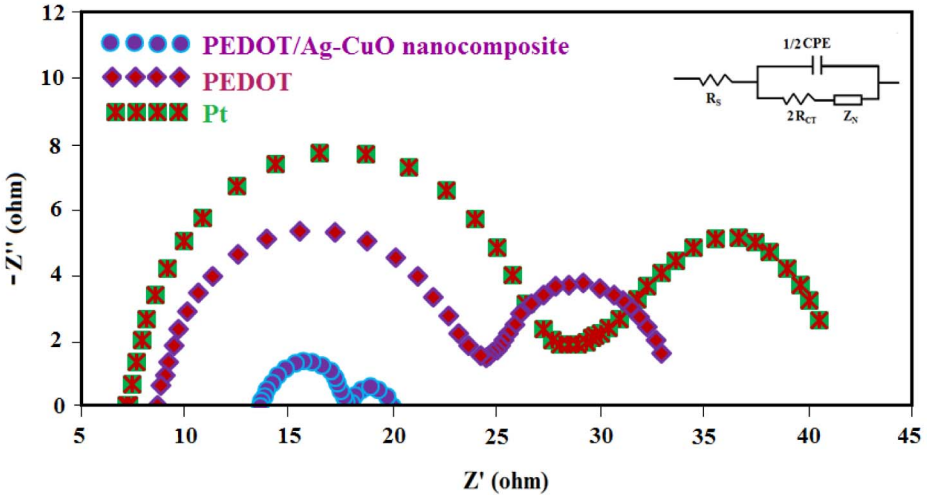

Figure 5. AC impedance measurements of the cell fabricated with two identical symmetric cells: Pt, PEDOT/Ag–CuO nanocomposite and PEDOT CEs at 1 sun illumination.

Table 1. Fitted impedance data of the Nyquist plots (R_S, R_{CT}, Z_N), and J_0 for DSSCs based on PEDOT, PEDOT/Ag–CuO nanocomposite and Pt counter electrodes

Counter electrode	R_S (Ω)	R_{CT} (Ω)	Z_N (Ω)	J_0 (mA/cm^2)
PEDOT/Ag–CuO nanocomposite	13.6	2.21	1.99	7.08
PEDOT	8.71	8.00	8.29	3.98
Pt	7.28	10.8	11.9	2.24

CE has a higher catalytic activity when compared to the conventional Pt CE. Furthermore, the limiting diffusion exchange current density (J_{lim}) can be determined from the Tafel polarization curve [26]. The novel PEDOT/Ag–CuO nanocomposite CE has a superior J_{lim}. The latter is directly proportional to the diffusion coefficient (D) [27]:

$$D = dJ_{lim}/2nFC, \quad (4)$$

where D and C are the diffusion coefficient and concentration of I_3^-; n is the number of electrons involved in the redox reaction; d and F are the distance between two electrodes and the Faraday constant, respectively. Therefore a better diffusion of the electrolyte through the photocathode can be inferred from a higher J_{lim} [25]. One can see that the J_{lim} value decreases in the following order PEDOT/Ag–CuO nanocomposite > PEDOT > Pt CE. Therefore the capability of iodine species to diffuse in PEDOT/Ag–CuO nanocomposite-based DSSCs is more notable than that in the other two CEs. The results from the Tafel plots are consistent with the CV studies.

3.5. *Alternating current impedance spectroscopy (ACIS)*

Figure 5 shows the Nyquist plots of platinum, PEDOT and the novel PEDOT/Ag–CuO nanocomposite-based CEs. Clearly, the decrease in the semicircle diameter at high frequency is attributed to the reduction of charge-transfer resistance at the photocathode and electrolyte interface. Actually, the I_3^- ions are reduced to I^- by the electrons coming from the TiO_2 semiconductor surface according to (2) ($I_3^- + 2e^- \rightarrow 3I^-$). The inset shows the equivalent circuit of different CEs. The charge-transfer resistance (R_{CT}) value is used to measure the catalytic activity; a lower R_{CT} signifies a higher ECA and vice versa [27]. The series resistance (R_S) was estimated from the intercept

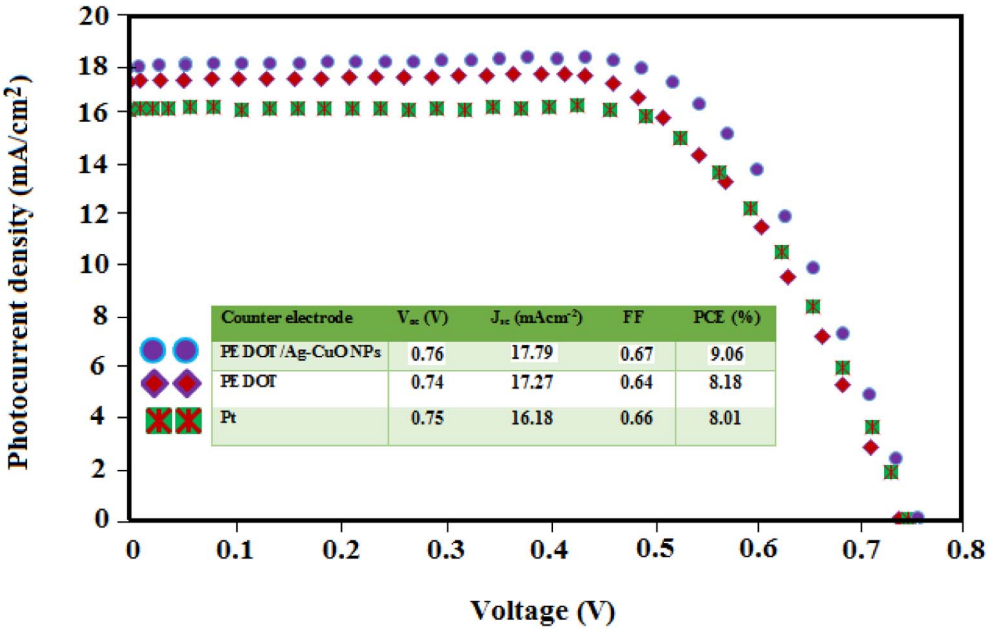

Figure 6. Photocurrent–voltage plots measured at 1 sun illumination of DSSCs including PEDOT, PEDOT/Ag–CuO nanocomposite and Pt CEs.

Table 2. Photovoltaic characteristics for DSSCs based on PEDOT, PEDOT/Ag–CuO nanocomposite and Pt CEs under 1 sun illumination (AM1.5, 100 mW/cm^2)

Counter electrode	V_{oc} (V)	J_{sc} (mA·cm^{-2})	FF	PCE (%)	J_{Red1} (mA/cm^2)	E_{pp} (mV)
PEDOT/Ag–CuO nanocomposite	0.76	17.79	0.67	9.06	−6.50	560
PEDOT	0.74	17.27	0.64	8.18	−5.20	590
Pt	0.75	16.18	0.66	8.01	−4.80	680

on the real axis in the left region, where R_S corresponds to the series resistance of the electrolyte and electrodes. The R_S values for PEDOT/Ag–CuO NPs CE (13.6 Ω), PEDOT (8.71 Ω) and platinum (7.28 Ω) are summarized in Table 1. A smaller value of R_{CT} (2.21 Ω) is also observed for PEDOT/Ag–CuO NPs CE in comparison with Pt (10.8 Ω), illustrating good ECA for the triiodide reduction in PEDOT/Ag–CuO nanocomposite based devices. This result is in agreement with the CV analysis. It was observed that PEDOT has a higher R_{CT} value than the PEDOT/Ag–CuO nanocomposite (8.00 Ω) due to low conductivity. However, after PEDOT is incorporated with Ag–CuO NPs, the R_{CT} value drops to 2.21 Ω, illustrating a faster electron transfer because of efficient charge dispersion. The investigation of the electrochemical behavior, including CV, Tafel polarization and ACIS, confirms that the PEDOT-based nanocomposite CE has greater ECA to reduce I_3^- to I^- in comparison with Pt-based devices. This is a result of electrical conductivity, which results from its unique porous network.

3.6. *Photocurrent density–voltage (J–V) measurements*

Figure 6 shows the photovoltaic characteristic of DSSCs prepared using platinum, PEDOT and the novel PEDOT/Ag–CuO nanocomposite as CEs at 1 sun (AM1.5). From the results (Table 2), the PEDOT CE device yields a PCE of 8.18%, with open-circuit voltage V_{OC} 740 mV, short-circuit current J_{SC} 17.27 mA/cm^2 and fill factor FF 0.64, which is

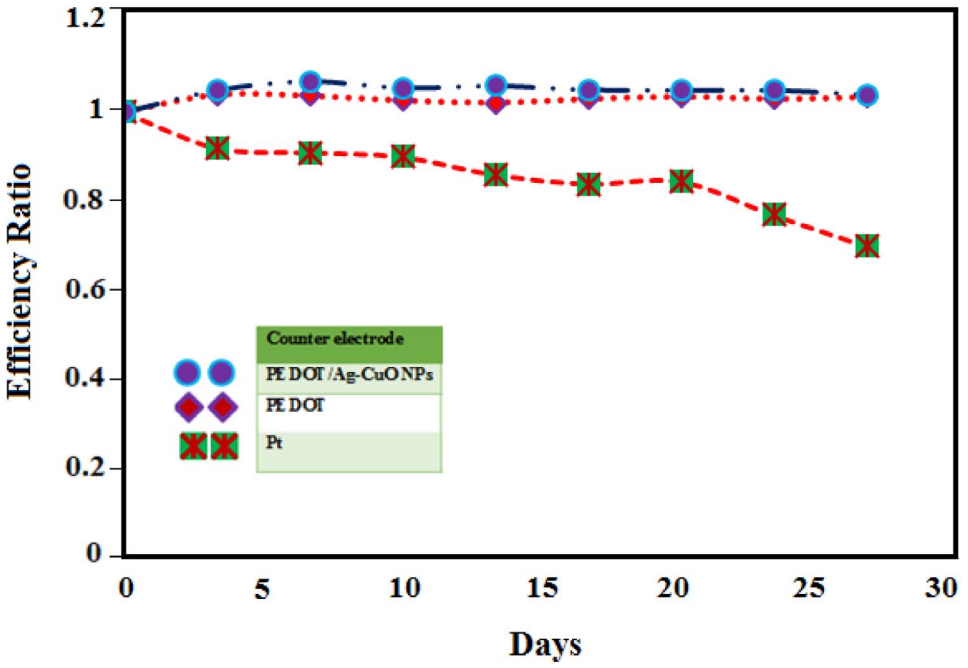

Figure 7. Long-term stability of DSSCs employing CEs with PEDOT/Ag–CuO nanocomposite (circle), PEDOT (diamond) and Pt (square).

lower than that of the PEDOT/Ag–CuO nanocomposite CE (PCE = 9.06%). The Pt CE system reaches a PCE of 8.01% with V_{OC} 750 mV, J_{SC} 16.18 mA/cm^2 and FF 0.66. Despite the excellent chemical stability and conductivity, PEDOT produces a low efficiency (8.18%) due to its small surface area [28] resulting in a low activity for I_3^- to I^- reduction. To overcome this problem, a high surface area nanocomposite material such as Ag–CuO is incorporated with PEDOT to achieve a higher performance. When it is compared to the PEDOT CE based DSSCs, the PCE of PEDOT/Ag–CuO nanocomposite CEs is noticeably improved by 10.76% due to the enhanced ECA, light scattering effect and higher conductivity of the novel CE. As a result, a PCE of 9.06% is achieved using the novel CE, which shows an improvement in PCE by 13.11% as compared to the Pt CE under the same conditions. As shown in the figure and the results summarized in Table 2, the solar cells based on PEDOT and Ag–CuO nanocomposite have the best performance in comparison with the other two CEs. Moreover, the novel PEDOT/Ag–CuO nanocomposite CE possesses a higher conversion efficiency of 9.06%, better electrochemical conductivity and ECA for I_3^- to I^- reduction when compared to the other Pt-free CEs [10,16,29].

3.7. *Long-term stability test of DSSCs based on different counter electrodes*

Figure 7 displays the long-term stability of cells fabricated with the different CEs. The changes in DSSC conversion efficiencies were monitored for 30 days. While the PEDOT/Ag–CuO and the PEDOT-based cells were stable for 30 days, the performance of the Pt-based cell drastically declined after only 10 days, indicating remarkable stability of PEDOT/Ag–CuO-based cells for long-term operation.

4. Conclusion

Recently, PEDOT-based materials have shown enormous promise in the field of new renewable energy sources because of their accessibility, easy production and cost-effectiveness. In this work, a novel PEDOT/Ag–CuO nanocomposite was prepared and used as the CE in DSSCs. The electrochemical behavior of the new device was influenced by the ECA

layer because it showed the combined effects of PEDOT, CuO and Ag nanoparticles. The photocurrent increased significantly in comparison with the cells with pristine Pt or PEDOT electrodes individually. Particularly, the novel PEDOT/Ag–CuO nanocomposite CE possesses higher photovoltaic conversion efficiency (9.06%), a low R_{CT} value (2.21 Ω) and effective electrochemical conductivity (PEDOT: high conductivity) and ECA to reduce I_3^- to I^- (Ag–CuO nanocomposite: high surface area).

Acknowledgments

The authors wish to thank the Yazd University Research Council, IUT Research Council and Excellence in Sensors for financial support of this research.

References

[1] J. Twidell, T. Weir, Renewable Energy Resources, Routledge, 2015.
[2] U. Bach, "Solid-state dye-sensitized mesoporous TiO_2 solar cells", Thesis No 2187, 2000.
[3] M. A. Green, Third Generation Photovoltaics, Springer, 2006.
[4] L. Wagner, *Analyst*, 2007, 1-15.
[5] M. Grätzel, *J. Photochem. Photobiol. C: Photochem. Rev.*, 2003, **4**, 145-153.
[6] B. E. Hardin, H. J. Snaith, M. D. McGehee, *Nat. Photonics*, 2012, **6**, 162.
[7] M. Mazloum-Ardakani, R. Arazi, *Heliyon*, 2019, **5**, e01444.
[8] H. Sun, L. Zhang, G. Zhou, Z. Wang, *Part. Part. Syst. Charact.*, 2016, **33**, 729-733.
[9] S. Sarker, K.-S. Lee, H. W. Seo, Y.-K. Jin, D. M. Kim, *Sol. Energy*, 2017, **158**, 42-48.
[10] M. Gao, Y. Xu, Y. Bai, S. Jin, *Appl. Surf. Sci.*, 2014, **289**, 145-149.
[11] H. Shirakawa, E. J. Louis, A. G. MacDiarmid, C. K. Chiang, A. J. Heeger, *J. Chem. Soc. Chem. Commun.*, 1977, 578-580.
[12] M.-H. Yeh, C.-P. Lee, C.-Y. Chou, L.-Y. Lin, H.-Y. Wei, C.-W. Chu, R. Vittal, K.-C. Ho, *Electrochim. Acta*, 2011, **57**, 277-284.
[13] M. Mazloum-Ardakani, R. Arazi, *Nanochem. Res.*, 2017, **2**, 20-28.
[14] M. Mazloum-Ardakani, R. Arazi, H. Beitollahi, H. Naeimi, *Anal. Methods*, 2010, **2**, 1078-1084.
[15] M. Mazloum-Ardakani, R. Arazi, *Anal. Bioanal. Electrochem.*, 2016, **8**, 675-690.
[16] Z. Pang, Y. Zhao, Y. Duan, J. Duan, Q. Tang, L. Yu, *J. Energy Chem.*, 2019, **30**, 49-56.
[17] K. Dhara, J. Stanley, T. Ramachandran, B. G. Nair, S. B. TG, *Sensors and Actuators B: Chem.*, 2014, **195**, 197-205.
[18] M. Mazloum-Ardakani, R. Arazi, F. Tamaddon, M. T. Kazemi, *Ionics*, 2017, **23**, 1591-1599.
[19] M. Mazloum-Ardakani, R. Arazi, M. Haghshenas, F. Tamaddon, M. Alizadeh, *Electrochim. Acta*, 2018, **266**, 452-459.
[20] J. Rodríguez-Moreno, E. Navarrete-Astorga, F. Martín, R. Schrebler, J. R. Ramos-Barrado, E. A. Dalchiele, *Thin Solid Films*, 2012, **525**, 88-92.
[21] D. M. Welsh, L. J. Kloeppner, L. Madrigal, M. R. Pinto, B. C. Thompson, K. S. Schanze, K. A. Abboud, D. Powell, J. R. Reynolds, *Macromolecules*, 2002, **35**, 6517-6525.
[22] F. Gong, H. Wang, X. Xu, G. Zhou, Z.-S. Wang, *J. Am. Chem. Soc.*, 2012, **134**, 10953-10958.
[23] Y. Zhao, J. Duan, Y. Duan, H. Yuan, Q. Tang, *Mater. Lett.*, 2018, **218**, 76-79.
[24] Y. Xiao, J.-Y. Lin, S.-Y. Tai, S.-W. Chou, G. Yue, J. Wu, *J. Mater. Chem.*, 2012, **22**, 19919-19925.
[25] M. Chen, L.-L. Shao, *Chem. Eng. J.*, 2016, **304**, 629-645.
[26] Y. Liao, K. Pan, L. Wang, Q. Pan, W. Zhou, X. Miao, B. Jiang, C. Tian, G. Tian, G. Wang, *ACS Appl. Mater. Interfaces*, 2013, **5**, 3663-3670.
[27] M. Mazloum-Ardakani, R. Arazi, B. B. F. Mirjalili, S. Azad, *Int. J. Energy Res.*, 2019, **43**, 4483-4494.
[28] D. H. Yoon, S. H. Yoon, K.-S. Ryu, Y. J. Park, *Sci. Rep.*, 2016, **6**, 19962.
[29] Q. Yang, J. Yao, K. Zhang, W. Wang, X. Zuo, H. Tang, M. Wu, G. Li, *J. Electroanal. Chem.*, 2019, **833**, 1-8.